Asociación Argentina
de Mecánica Computacional

Mecánica Computacional Vol XXXV, págs. 953-963 (artículo completo)
Martín I. Idiart, Ana E. Scarabino y Mario A. Storti (Eds.)
La Plata, 7-10 Noviembre 2017

DIRECT NUMERICAL SIMULATION OF SECONDARY FLOW IN STRAIGHT DUCTS FORCED BY NON-HOMOGENOUS FORCE

Julia V. Martorana[a,b] **and Mariano I. Cantero**[a,b,c]

[a]*Centro Atómico Bariloche, Comisión Nacional de Energía Atómica, San Carlos de Bariloche, Río Negro, Argentina, julia.martorana@cab.cnea.gov.ar, http://mecom.cnea.gov.ar/.*

[b]*Instituto Balseiro, San Carlos de Bariloche, Río Negro, Argentina.*

[c]*Consejo Nacional de Investigaciones Científicas y Técnicas, San Carlos de Bariloche, Río Negro, Argentina.*

Keywords: secondary flow, duct, DNS, turbulent flow

Abstract. Turbulent flow in ducts of rectangular section presents secondary flows due to the presence of turbulence. In this work we study this kind of turbulent flow driven by a non-uniform force in the vertical direction. This kind of forcing is used to model the stratification effect over the driving force of the flow. Of particular interest to this work are gravity currents, which are stratified flows generated by the gravity action over relatively small differences in density between two fluids. The fact that the flow is forced by the action of gravity on the density profiles causes the stratification effects to appear on two very different scales. On the microscopic scale stratification modulates turbulence and on the macroscopic scale stratification modulates the driving force of the flow. The objective of this work is to analyze separately the macroscopic effect of stratification inhibiting completely the microscopic effect of stratification. In this work, variations produced on secondary flow of the second kind when the flow is driven by forces that vary linearly and exponentially in the vertical direction are analyzed. These results are compared with the case of flow driven by an uniform force in the vertical direction. To this aim fully resolved direct numeric simulations are performed with a pseudo-spectral code.

1 INTRODUCTION

The secondary flow presents in the turbulent flow in straight ducts is generated only due to the presence of turbulence. This kind of flow was classified by Prandtl (1926) as secondary flow of the second kind. The secondary flow of the first kind, however, can be arised in both laminar and turbulent flows and it is generated by the skewness of the vorticity vector (Bradshaw, 1987).

Although the secondary flow of the second kind can only reach values of approximately 2-3% of the main velocity, its effects can be important. This secondary flow increases wall shear stresses and this is significant in problems of sediment transport and erosion (Abad et al., 2013). Similarly, heat transfer and contaminants dispersion are affected by the secondary flows (Simpson, 1997). For these reasons it is important to understand the behavior of the secondary flow and to achieve precise prediction of this phenomena.

Many works concerning with this kind of secondary flow can be found in the literature. The first works that presents Direct Numerical Simulation (DNS) (Gavrilakis, 1992; Huser and Biringen, 1993) analyze the origin and behavior of the secondary flow. More recently works show the influence of the Reynolds number in the mean flow (Pinelli et al., 2010; Zhang et al., 2015) and the effect of the duct section aspect-ratio (Vinuesa et al., 2014), all of them using DNS. Regarding to Large Eddy Simulations (LES), the works of Madabhushi and Vanka (1991); Yao et al. (2015) and Breuer and Rodi (1994) can be mentioned. In these studies the analysis of the characteristics of the flow for different Reynolds numbers is also carried out. Among the experimental studies, the works of Brundrett and Baines (1964); Launder and Ying (1972) and Melling and Whitelaw (1976) can be found for high Reynolds numbers ($Re_b > 35000$; where $Re = u_b h/\nu$, where u_b is the bulk velocity, h is the half-width of the duct and ν is the kinematic viscosity). For low Reynolds number the works of Kawahara et al. (2000) ($Re_b = 3535$) and Owolabi et al. (2016) ($Re_b = 1203$ y 2230) can be referred to.

Stratified flows are those in which the density varies in the vertical direction. Gravity currents, in particular, are stratified flows generated by the gravity action over relatively small differences in density between two fluids (García, 1992). In these flows the action of gravity on the density profiles causes the stratification effects to appear on two very different scales. On the microscopic scale stratification modulates turbulence and on the macroscopic scale stratification modulates the forcing of the flow.

Turbidity currents are flows in which the variation of the density occurs by solids in suspension due to the action of gravity. The sediment interacts with the flow changing its turbulent structure and, in consequence, modifying the solid phase-ambient fluid turbulent mixing and the velocity and concentration profiles. In this direction, Armenio and Sarkar (2000) made LES simulations of a stably-stratified flow in a channel and observed that an increase in the stratification causes a systematic reduction of the turbulence levels, density fluctuations and associated vertical transport. Furthermore, Cantero et al. (2009a,b) and Shringarpure et al. (2010, 2014, 2015) performed DNS simulations of a self-stratified turbulent flow forced by suspended sediments and showed that the self-stratification of the flow decrease the turbulence, in particular, near the bottom of the channel. In these works both the microscopic stratification effect on the modulating of the turbulence and the macroscopic stratification effect on the driving force are studied and the individual impact of each effect can't be identified.

In this work secondary flow of the second kind generated by turbulent flow in a duct of square section is studied. To model the macroscopic stratification effect separately, a non-uniform force in the vertical direction is used to drive the flow. In a previous work (Martorana et al. (2016)) linear variations of the driving force were imposed with this aim. In this study,

variations produced on secondary flow of the second kind when the flow is driven by forces that vary linearly and exponentially in the vertical direction are analyzed. These results are compared with the case of flow driven by an uniform force in the vertical direction. For this purpose, fully resolved direct numeric simulations are performed with a pseudo-spectral code that uses Fourier expansions for the flow direction and Chebyshev expansions for the remaining directions. Results on the variations in the mean flow, in secondary flow and in turbulence are reported.

2 MATHEMATICAL AND NUMERICAL MODEL

In this work an incompressible flow in a straight duct driven by a force in the streamwise (x) direction is considered. The flow is governed by the dimensionless equations

$$\frac{\partial \tilde{\mathbf{u}}}{\partial \tilde{t}} + \tilde{\mathbf{u}} \cdot \nabla \tilde{\mathbf{u}} = -\nabla \tilde{p} + \frac{1}{Re_\tau} \nabla^2 \tilde{\mathbf{u}} + \mathbf{F}, \qquad \nabla \cdot \tilde{\mathbf{u}} = 0 \tag{1}$$

where $\tilde{\mathbf{u}} = \{\tilde{u}, \tilde{v}, \tilde{w}\}$ is the dimensionless velocity, $\tilde{p}$ is the dimensionless pressure and $\mathbf{F}$ is the non-uniform force in the vertical direction that forces the flow in the streamwise direction (x) ($\mathbf{F} = \{F_x(y), 0, 0\}$). The dimensionless equations 1 are obtained using the friction velocity $u_\tau = \sqrt{\tau_w/\rho}$ as the velocity scale, where τ_w is the wall shear stress and ρ is the fluid density. The semiwidth h is taken as the length scale, $T = h/u_\tau$ is used for temporal scale and ρU^2 is chosen for pressure scale. The flow depends on the Reynolds number $Re_\tau = u_\tau\, h/\nu$, where ν is the fluid kinematic viscosity.

The dimensionless equations in 1 are solve using a pseudo-spectral code (Canuto et al., 1988). This code employs Fourier expansions in the streamwise direction (x) and Chebyshev expansions with Gauss-Lobato quadrature points in the remaining directions ($z - y$). The fractional step method (Kim and Moin, 1985) is used to solve the momentum equation and the incompressibility condition. A third order Adams-Bashforth and a Crank-Nicolson scheme is used for temporal discretization of the advection and diffusive terms respectively. The solutions of the discretisized partial differential equations are obtained by means of a fast 2D Helmholtz solver. Details of the calculation process of this code can be found in the work of Martorana et al. (2016) .

The dimensions of the duct employed for the simulations are $L_x \times L_y \times L_z = 4\pi h \times 2h \times 2h$. The streamwise length can be considered sufficiently long in order to allow an adequate decay of the two-point velocity correlations according to Gavrilakis (1992) and Pinelli et al. (2010). The grid resolution used is $(N_x, N_y, N_z) = (131, 131, 192)$. Periodic boundary conditions are enforced along the streamwise direction (x) for all variables. For the four walls of the duct the no-slip boundary condition is enforced for the streamwise velocity. For the horizontal velocity w (vertical velocity v) no-slip boundary condition is imposed in the horizontal walls (vertical walls) and the condition of no-penetration in the vertical walls (horizontal walls). The initial condition used for the velocity field is taken from a fully developed turbulent open channel flow solution.

3 RESULTS

The behavior of the secondary flow generated in a flow with non-homogeneous forcing in the vertical direction is studied. This analysis is perform for several linear and exponential

variations in the vertical direction as it is shown in table 1. These variations are given by

$$\begin{aligned} F_x &= \beta(1-y)+2, \quad \text{for CC y CL,} \\ F_x &= \frac{-4\beta}{e^{-2\beta}-1}e^{-\beta y}, \quad \text{for CE} \end{aligned} \tag{2}$$

where the coefficient values β are listed in the table 1. For the studied cases

$$\int_0^2 F_x dy = 4 \tag{3}$$

and the net forcing of the flow is the same for all cases. The statistics of the mean flow was obtained by averaging both in the time and in the flow direction the instant values. For the cases CL and CE the averaging was also made between the two vertical halves taking advantage of the symmetry of the problem. The integration time was of 600 time units. Additionally, the bulk velocity u_b, the Reynolds number based on the bulk velocity $Re_b = u_b h/\nu$, the position of the maximum value of main velocity at the vertical center line of the section $y_{u,max}$ and the local friction velocity at the center of the walls ($u_{\tau,t}$ for top wall, $u_{\tau,b}$ for bottom wall, $u_{\tau,h}$ for horizontal walls) are exhibited in table 1.

Caso	β	$u_b/u_{\tau,avg}$	Re_b	$y_{u,max}$	$u_{\tau,t}$	$u_{\tau,b}$	$u_{\tau,h}$
CC	0.0	15.12	2721	1.00	1.072	1.072	1.072
CL1.5	1.5	14.90	2683	0.86	1.026	1.010	1.070
CL2	2.0	14.72	2650	0.81	1.016	0.982	1.061
CE3	3.0	13.63	2381	0.36	0.869	1.225	0.909
CE5	5.0	11.98	2157	0.22	0.789	1.374	0.824

Table 1: Cases studied in this work

Driving force variations in the vertical direction are shown in figure 1. The driving forces imposed in this study are similar to the density profiles of the turbidity currents. This kind of forcing is used to modelate the stratification effect on the forcing of the flow separately.

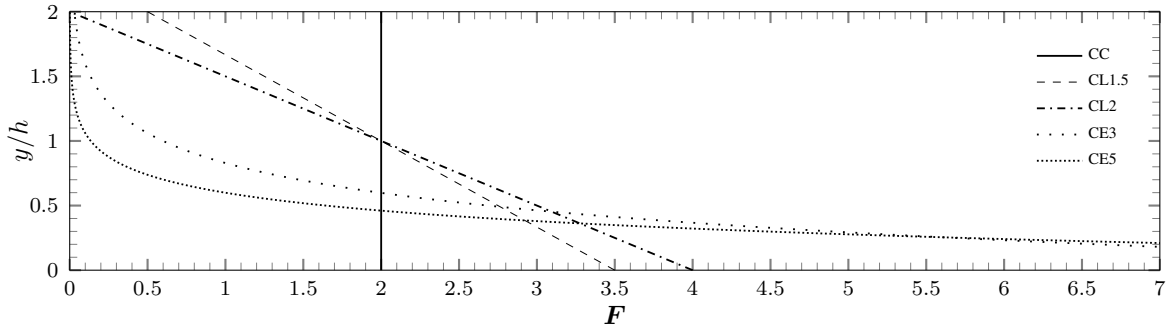

Figure 1: Vertical variation of the imposed forces for the studied cases.

Figure 2 shows vertical variation of the main velocity normalized with the main bulk velocity in two lines of the section. Figure 2(a) presents the variation at $z/h = 0.5$ and figure 2(b) exhibits the profile at $z/h = 1$. It can be seen in both lines that the position of the maximum values of main velocity decrease in all the studied cases compared with the base case (case

CC). In particular, for the linear variation cases (cases CL) these maximum are located near the maximum value of case CC. For cases with exponential variations (cases CE), instead, a bigger descend of these values can be observed, being located near the horizontal bottom wall. The positions of the maximum values at the center line of the section (figure 2(b)) for each case are presented in table 1. The descend of the maximum values is higher at $z/h = 0.5$ than at the center line of the section. With regard to the magnitude of velocity, an increment in the lower half of the section and a decrease in the upper half of the section can be identified compared with the base case. The maximum values of velocity are higher at the center line of the section.

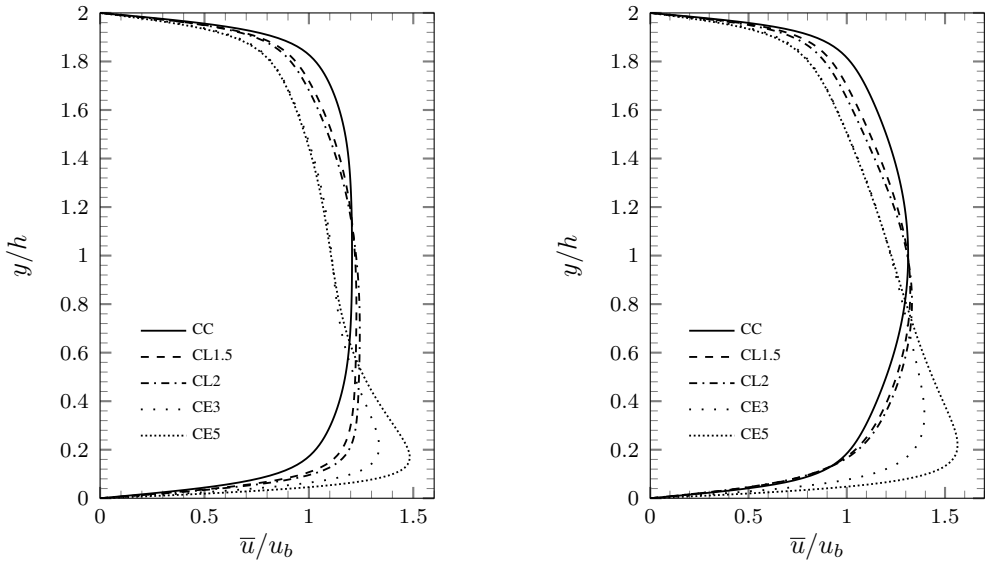

Figure 2: Vertical variation of the streamwise velocity. (a) At $z/h = 0.5$. (b) At $z/h = 1$

The variations of the main velocity at horizontal lines are presented in figure 3. As it can be seen in figure 2, the main velocity decreases with respect to case CC at the upper region of the section (figure 3(a)) and increases at the bottom region (figure 3(c)). At the upper line $y/h = 1.5$ the variation is similar between cases CL and is practically the same for cases CE. The profiles are constants at the central third of the section. At the horizontal center line of the section (figure 3(b)), the profiles for cases CL are very similar to the base case, while the values of velocity for cases CE are lower than the values for case CC. Cases CE show the same variation of velocity between each other along the center line. At the lower part of the section ($z/h = 0.5$, figure), the velocity profiles for cases CE present a significant increase at the center region of the section compared to case CC.

The profiles for the vertical secondary velocity $\overline{v}$ in two vertical lines, $z/h = 0.5$ and $z/h = 1$ are shown in figure 4. The variation across the line $z/h = 0.5$ presents an increase of the velocity in the central zone of the section with respect the base case and a decrease in the lower third of the section. On the other hand, at the center line of the section $z/h = 1$, an increase in the lower third of the section can be observed for cases CL and a significant increment in the central third of the section for cases CE. The maximum values are higher for cases CE than for cases CL.

With regard to the horizontal secondary velocity $\overline{w}$, the profiles across the horizontal lines $z/h = 1.5$, $z/h = 1$ and $z/h = 0.5$ are presented in figure 5. At the upper region of the section

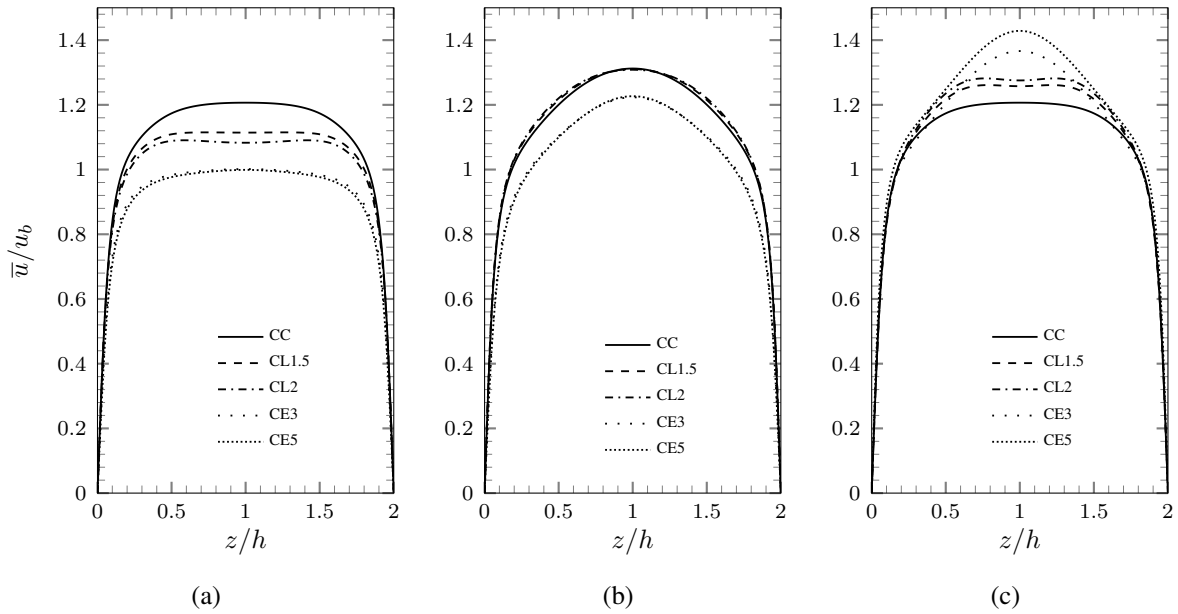

Figure 3: Horizontal variation of the streamwise velocity. (a) At $y/h = 1.5$. (b) At $y/h = 1$. (c) At $y/h = 0.5$

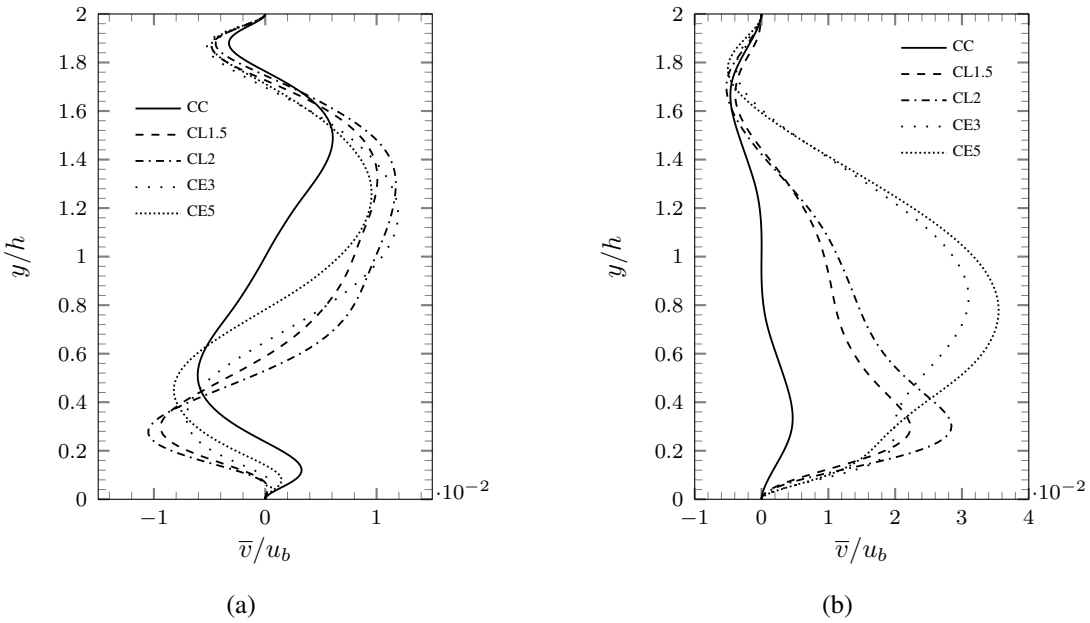

Figure 4: Vertical variation of the vertical velocity $\overline{v}$. (a) At $z/h = 0.5$. (b) At $z/h = 1$

(figure 5(a)), changes of sign near the vertical walls are not produced compared to case CC for cases CL and CE. At both lateral regions of the section, the velocities intensify with respect of case CC. These values are higher for cases CE than for cases CL. At the horizontal center line of the section (figure 3(b)) at each vertical half, changes in the sign for the studied cases compared to case CC can be observed. These profiles show higher values for cases CE than for cases CL. At the lower region of the section (figure 3(c)) the changes in the sign that present both CC and CL cases, are not produced for cases CE, in which at each vertical half of the section, the horizontal secondary velocity preserves the sign.

Figure 6 presents the total shear stress profiles in the vertical direction $\tau_{tot,y} = -\overline{u'v'} + \frac{1}{Re_\tau}\frac{\partial \overline{u}}{\partial y}$

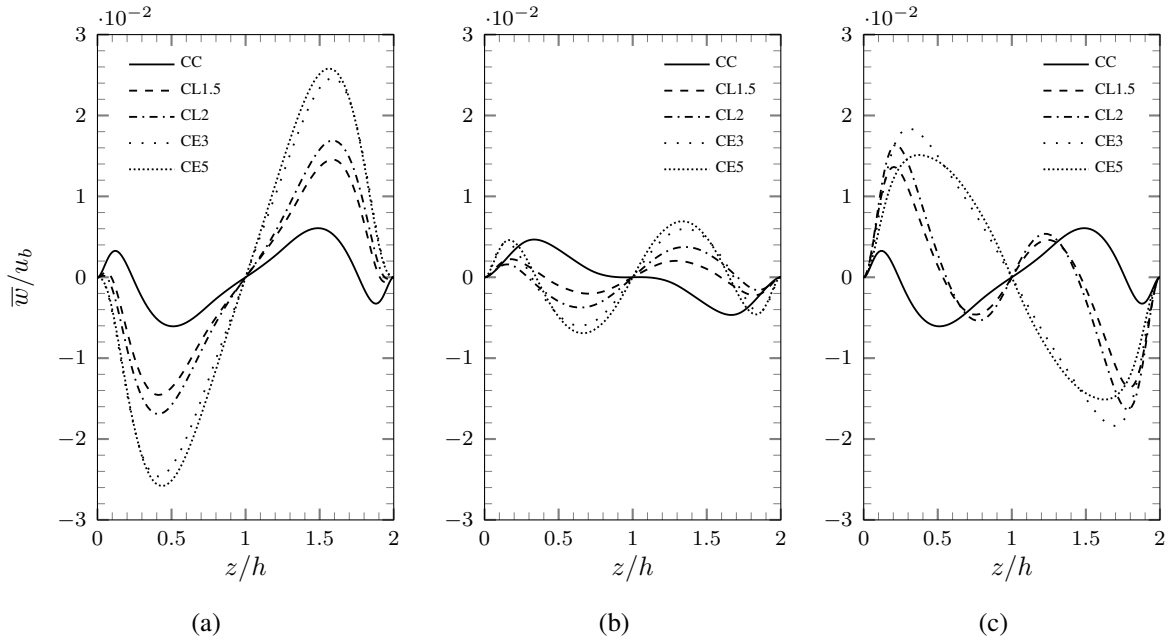

Figure 5: Horizontal variation of the horizontal velocity $\overline{w}$. (a) At $y/h = 1.5$. (b) At $y/h = 1$. (c) At $y/h = 0.5$

(figure 6(a)), the Reynolds stress (figure 6(b)) and the viscous stress (figure 6(c)) normalized with the local friction velocity at the center of the bottom wall for the studied cases. In both cases CL and CE the zero-value point of $\tau_{tot,y}$ descends towards the bottom wall. However, while in cases CL these points are located at the center region of the section, in cases CE these points move to the lower third of the section. In the lower half both values for cases CE and CL decrease compared with case CC, while at the upper half of the section, the values of cases CL increase in magnitude and the values for cases CE decrease in magnitude with regard to the base case. These variations are owed almost exclusively to the modifications of the Reynolds stress $-\overline{u'v'}$ as it can be seen in figures 6(b) and 6(c). The latter figure shows that the variations with respect to case CC are small.

If, instead, the corresponding local velocity friction value is used to normalized the variables at each half of the section, figure 7 is obtained. The values at the upper half of the section are normalized with the value of the friction velocity at the center of the upper wall $u_{\tau,t}$ and the lower half is normalized with the value of friction velocity at the center of the lower wall $u_{\tau,b}$. In this case, a different behavior at each vertical half of the section can be observed. The modifications of the total shear stress $\tau_{tot,y}$, owing mainly to the variations of the Reynolds stress $-\overline{u'v'}$ (figures 7(a) and 7(b)), show a decrease of the values at the lower half of the section and an increase in the magnitude at the upper half of the section. The decrease represents an attenuation of the turbulence due to the imposed forcing to the flow. The values at the upper half, on the contrary, indicate an intensification of the turbulence.

The rms values for each velocity component $u_{rms} = \overline{u'^2}^{1/2}$, $v_{rms} = \overline{v'^2}^{1/2}$ y $w_{rms} = \overline{w'^2}^{1/2}$ at the vertical center line normalized at the lower half of the section with the local friction velocity at the center of the bottom wall and in the upper half with the local friction velocity at the center of the top wall are shown in figure 8. At the lower part of the section, while cases CL present similar profiles compared to case CC, cases CE show a different behavior. The maximum values decrease and the profiles become more flatted at the most part of the lower half of the section. At the upper half of the section, the profiles for all the studied cases show an increment with

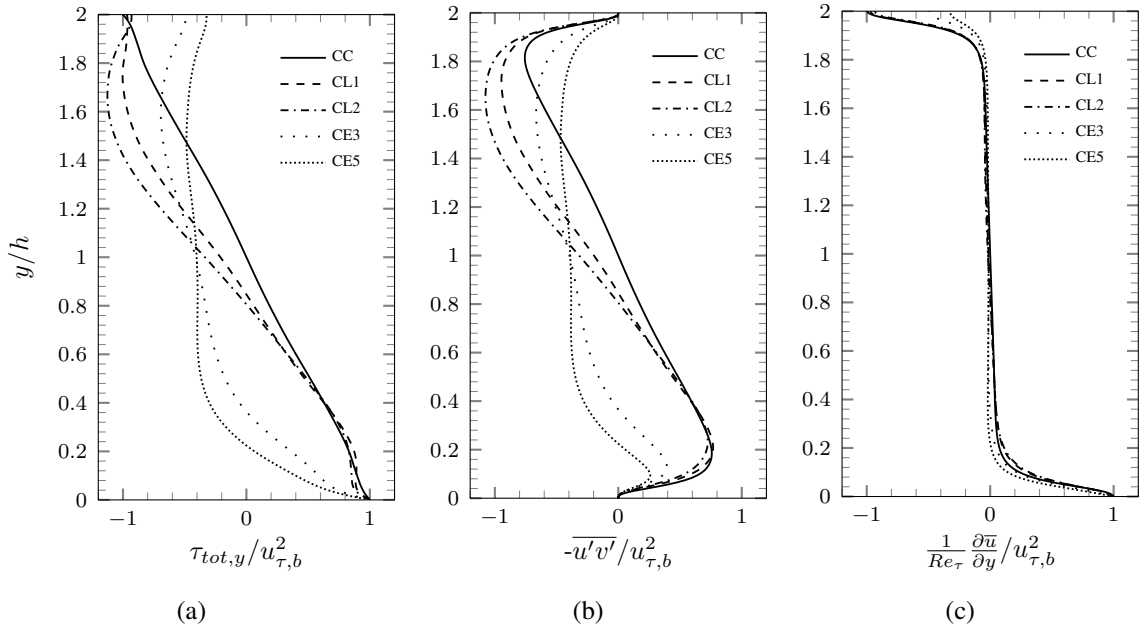

Figure 6: Profiles at $z/h = 1$. (a) Total vertical shear stress $\tau_{tot,y}$. (b) Reynolds stress $-\overline{u'v'}$. (c) Velocity gradient $\frac{1}{Re_\tau}\frac{\partial \overline{u}}{\partial y}$. All the values are normalized with local friction velocity at the center of the bottom wall $u_{\tau,b}$.

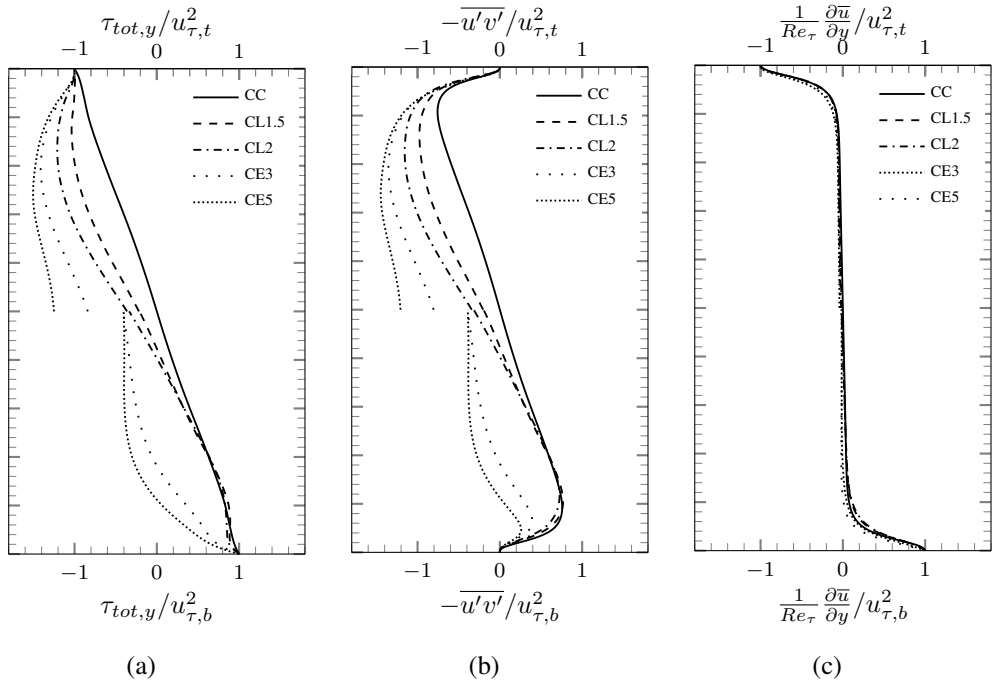

Figure 7: Profiles at $z/h = 1$. (a) Total vertical shear stress $\tau_{tot,y}$. (b) Reynolds stress $-\overline{u'v'}$. (c) Velocity gradient $\frac{1}{Re_\tau}\frac{\partial \overline{u}}{\partial y}$. The values from the upper half are normalized with local friction velocity at the center of the upper wall $u_{\tau,t}$ and the values from the bottom half are normalized with local friction velocity at the center of the bottom wall $u_{\tau,b}$

respect to the base case. In particular, cases CE present flatter profiles than cases CL as a bigger increment occurs at the central region of the section. The decrease of the maximum values of u_{rms} shows an attenuation of the turbulence at the lower third of the section. The increase in the

upper region is related with the increment of vertical momentum flux in that part of the section. The transverse rms values also exhibit variations that represent an attenuation of the turbulence at the lower third of the section and an increase in the upper region.

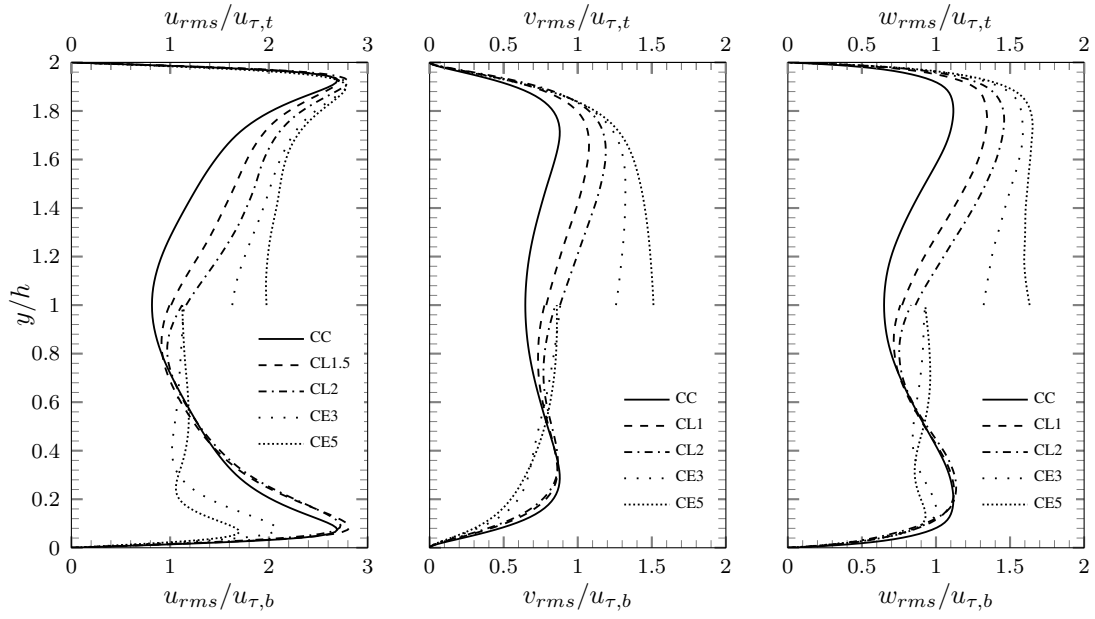

(a) (b) (c)

Figure 8: Profiles of rms values at $z/h = 1$. (a) u_{rms}. (b) v_{rms}. (c) w_{rms}. The values from the upper half are normalized with local friction velocity at the center of the upper wall $u_{\tau,t}$ and the values from the bottom half are normalized with local friction velocity at the center of the bottom wall $u_{\tau,b}$

4 CONCLUSIONS

In this work the secondary turbulent flow generated in a turbulent flow in a straight duct of square section is analyzed. The flow is forced by a non-uniform force in the vertical direction. The imposing of linear and exponential forces is used to model the macroscopic stratification effect separately.

Regarding the effects over the flow main velocity, it can be observed that the values increase at the lower half of the section and decrease at the upper half compared to case CC. These variations are more significant for cases CE than for cases CL. Also, even though the position of the maximum move towards the bottom wall for both cases CL and CE, for cases CE these values are located in the lower third of the section while for cases CL the position of the maximum remains at the center region of the section.

The components of the secondary velocity show an increase in magnitude and changes of the signs compared to case CC for both cases CL and CE. Cases CE shows higher values than cases CL.

The parameters related with turbulence also show variations compared with case CC. Both the Reynolds shear stress $-\overline{u'v'}$ and the rms values for all the studied cases present an increase at the upper half section. At the lower half of the section, cases CL exhibits similar profiles than case CC while cases CE present lower values than case CC. The reductions of these parameters show an attenuation of the turbulence at the bottom region and the increments at the upper half of the section represent an intensification of the turbulence.

REFERENCES

Abad J.D., Frias C.E., Buscaglia G.C., and Garcia M.H. Modulation of the flow structure by progressive bedforms in the Kinoshita meandering channel. *Earth Surface Processes and Landforms*, 38:1612–1622, 2013.

Armenio V. and Sarkar S. An investigation of stably stratified turbulent channnel flow using large-eddy simulation. *Journal of Fluid Mechanics*, 66:95–102, 2000.

Bradshaw P. Turbulent secondary flows. *Annual Review of Fluid Mechanics*, 19:53–74, 1987.

Breuer M. and Rodi W. Direct and large eddy simulation I. In P.R. Voke and J. Kleiser L. Chollet, editors, *ERCOFTAC Workshop on Direct and Large-Eddy Simulation*, pages 273–285. Kluwer Academic Publishers, 1994.

Brundrett E. and Baines W.D. The production and diffusion of vorticity in a square duct. *Journal of Fluid Mechanics*, 19:375–394, 1964.

Cantero M.I., Balachandar S., Cantelli A., Pirmez C., and Parker G. Turbidity current with a roof: Direct numerical simulation of self-stratified turbulent channel flow driven by suspended sediment. *Journal of Geophysical Research*, 114, 2009a.

Cantero M.I., Balachandar S., and Parker G. Direct numerical simulation of stratification effects in sediment-laden turbulent channel flow. *Journal of Turbulence*, 10:1–28, 2009b.

Canuto C., Hussaini M., Quarteroni A., and Zang T. *Spectral methods in fluid dynamics*. New York: Springer-verlag, 1988.

García M.H. Turbidity currents. In L. Brekhovskikh, K. Turekian, K. Emery, and C. Tseng, editors, *Encyclopedia of Earth System Science*, volume 4, pages 399–408. Academic Press, Inc., New York., 1992.

Gavrilakis S. Numerical simulation of low-reynolds-number turbulent flow through a straight square duct. *Journal of Fluid Mechanics*, 244:101–129, 1992.

Huser A. and Biringen S. Direct numerical simulation of turbulent flow in a square duct. *Journal of Fluid Mechanics*, 257:65–95, 1993.

Kawahara G., Ayukawa K., Ochi J., Ono F., and Kamada E. Wall shear stress and reynolds stresses in a low reynolds number turbulent square duct flow. *Trans JSME B*, 66:95–102, 2000.

Kim J. and Moin P. Application of a fractional step method to incompressible navier-stokes equations. *Journal of Computational Physics*, 59:308–323, 1985.

Launder B.E. and Ying W.M. Secondary flows in ducts of square cross-section. *Journal of Fluid Mechanics*, 54:289–295, 1972.

Madabhushi R.K. and Vanka S.P. Large eddy simulation of turbulence-driven secondary flow in a square duct. *Journal of Physics Fluids*, A3 11:2734–2744, 1991.

Martorana J.V., Cantero M.I., and Dari E.A. Simulación directa de turbulencia de flujo secundario en ductos rectos con gradientes de presión no uniformes. *Mecánica Computacional*, XXXIV:2137–2153, 2016.

Melling A. and Whitelaw J. Turbulent flow in a rectangular duct. *Journal of Fluid Mechanics*, 78:289–315, 1976.

Owolabi B.E., Poole R.J., and Dennis D.J.C. Experiments in low-reynolds-number turbulent flow through a square duct. *Journal of Fluid Mechanics*, 798:398–410, 2016.

Pinelli A., Uhlmann M., Sekimoto A., and Kawahara G. Reynolds number dependence of mean flow structure in square duct turbulence. *Journal of Fluid Mechanics*, 644:107–122, 2010.

Prandtl L. Über die ausgebildete turbulenz. *Verh. 2nd Intl Kong. für Tech. Mech., Zurich (English transl. NACA Tech. Memo 62, 435*, 1926.

Shringarpure M., Cantero M.I., and Balachandar S. Dynamics of complete turbulence suppression in turbidity currents driven by monodisperse suspensions of sediment. *Journal of Fluid Mechanics*, 712:384–417, 2010.

Shringarpure M., Cantero M.I., and Balachandar S. Mechanisms of complete turbulence suppression in turbidity currents driven by mono-disperse and bi-disperse suspensions of sediment. *Journal of Computational Multiphase Flows*, 6(3):16–23, 2014.

Shringarpure M., Cantero M.I., and Balachandar S. Analysis of turbulence suppression in sediment-laden saline currents. *Procedia Engineering*, 126:16–23, 2015.

Simpson J.E. *Gravity Currents in the environment and the laboratory*. Cambrigde University Press, 1997.

Vinuesa R., Noorani A., Lozano-Durán A., El Khoury G.K., Schlatter P., Fischer P.F., and Nagib H.M. Aspect ratio effects in turbulent duct flows studied through direct numerical simulation. *Journal of Turbulence*, 15:677–706, 2014.

Yao J., Zhao Y., and Fairweather M. Numerical simulation of turbulent flow through a straight square duct. *Applied Thermal Engineering*, 91:800–811, 2015.

Zhang H., Trias F.X., Gorobets A., Tan Y., and Oliva A. Direct numerical simulation of a fully developed turbulent square duct flow up to Re_τ. *Journal of Heat and Fluid Flow*, 54:258–267, 2015.